Ab initio thermo-elasticity of -MH **(M=Zr, Ti)**

Olsson, Pär

Published in:
Computational Materials Science

DOI:
10.1016/j.commatsci.2022.111953

2023

Document Version:
Publisher's PDF, also known as Version of record

Computational Materials Science 218 (2023) 111953

Contents lists available at ScienceDirect

Computational Materials Science

journal homepage: www.elsevier.com/locate/commatsci

Full length article

Ab initio thermo-elasticity of δ-MH_x (M=Zr, Ti)

Pär A.T. Olsson *

Materials Science and Applied Mathematics, Malmö University, SE 205 06 Malmö, Sweden
Division of Mechanics, Materials and Components, Lund University, Box 118, SE 221 00 Lund, Sweden

ARTICLE INFO

Keywords:
Zirconium hydride
Titanium hydride
Thermo-elasticity
Ab initio density functional theory

ABSTRACT

In the present work, we report the results of a systematic *ab initio* study of the thermo-elastic properties of δ-$MH_{1.5}$ (M=Zr, Ti). This investigation serves three purposes: (i) Elucidate the fully anisotropic temperature dependent elastic constants of hydrides, (ii) address discrepancies in thermal expansion data reported in the literature and (iii) provide input data for thermodynamic-based phase-transformation modelling. Due to a reduced contribution from the vibrational free energy to the strain energy, in agreement with experimental observations we find that the temperature dependent stiffness of hydrides vary to a much lesser degree than the matrix. For δ-$ZrH_{1.5}$, we further find that Zener's anisotropy ratio varies with temperature. Regarding the linear thermal expansion, our results indicate that it is highly temperature dependent. With the exception of a few outliers, our DFT data concurs well with experimental data, if the temperature range over which it was measured is taken into account.

1. Introduction

The group IVB transition metals, zirconium (Zr) and titanium (Ti), possess several beneficial properties, which make them attractive for a multitude of applications, including nuclear fuel cladding [1] and light-weight applications, such as airframes and components in aerospace engines [2–4]. The Zr-H and Ti-H phase diagrams are similar: at low temperature and pressure the ground-state structure corresponds to hexagonal close-packed (HCP), which has a low solubility limit for hydrogen above which they form hydrides [5,6]. The formation of such hydrides, which are inherently brittle, can have a detrimental effect on the integrity and longevity for components operating hydrogen-rich environments. It can give rise to phenomena, such as delayed hydride cracking in Zr alloys [7] or sustained load cracking in Ti alloys [8], which yield reduced load-carrying capability and promote premature failure. This becomes especially important in the proximity of local stress concentrations, such as notches, dislocations or crack-tips, since they may facilitate hydride formation [9,10].

There are two well-established hydride morphologies for both Ti and Zr: at high hydrogen content the ϵ-MH_2 (M=Zr, Ti) forms, which is a stoichiometric face-centred tetragonal phase, while at lower hydrogen content the non-stoichiometric δ-MH_x phase is formed. The latter is a face-centred cubic (FCC) phase with hydrogen in the range of concentration corresponding to $1.4 \lesssim x \lesssim 2$ randomly occupying tetrahedral interstitial sites [5,6,11,12]. Beside these phases there is a number of controversial phases, whose stability is subject to debate. They include γ-MH, whose formation is dependent on the cooling rate. There are, however, contradicting findings in experiments [13] and modelling efforts [14] in the literature: experiments indicate that γ preferentially forms during fast cooling [13], whereas predictions from *ab initio*-based modelling suggest that it forms under slow cooling [14]. Moreover, there is the ξ-M_2H phase, which is fully coherent with the matrix and is believed to be an intermediate transitional phase between α and δ or γ [11,12,15].

To model the formation of secondary phases, different types of thermodynamic-based modelling approaches have emerged. Notably, variants of phase-field and continuum modelling have been extensively used to investigate aspects such as hydride formation and reorientation under applied load [16–19], and formation and fracture in the proximity of stress concentrators [20–24]. The predictability of such modelling relies heavily on the accuracy of the free energy functional and its ability to account for aspects such as e.g. chemical, interfacial and elastic free energy. Since all hydride phases form with preferential orientations relative to the matrix, see e.g. [13], anisotropic thermo-elastic contributions to the free energy description are necessary to capture thermally-induced variations in stiffness and lattice mismatch between phases.

Experimental investigations have shown that Young's modulus and the hardness of α-Zr reduce faster with increasing temperature than for hydrides [25,26], indicating that the divergence in mechanical properties between the two is highly temperature dependent. There is a lack of experimental data concerning the anisotropic elastic constants

* Correspondence to: Materials Science and Applied Mathematics, Malmö University, SE 205 06, Malmö, Sweden.
E-mail address: Par.Olsson@mau.se.

https://doi.org/10.1016/j.commatsci.2022.111953
Received 14 September 2022; Received in revised form 15 November 2022; Accepted 27 November 2022

of hydride phases. Although they have been computed by several investigators at $T = 0$ K by means of *ab initio* ground-state density functional theory (DFT) modelling, see e.g. [27–37], currently it is unknown how they vary with temperature. To capture such behaviour by means of DFT it is necessary to go beyond ground-state modelling and include entropic contributions to the free energy through e.g. the quasi-harmonic approximation (QHA), in which the vibrational free energy emanating from phonon excitations are incorporated [38]. Owing to the much increased computational effort required for such modelling, only relatively few efforts have been directed towards computing temperature dependent elastic constants. They have mostly been limited to FCC [39–41], HCP [40,42,43], diamond [44] and body-centred cubic crystals [45,46], while only few works have addressed more complex ceramics [47,48]. But to the best of the author's knowledge, no efforts have been directed towards elucidating the thermal dependence of the elastic constants of hydrides. This lack of data limits the prospect of formulating temperature dependent free energy functionals for phase-transformation modelling.

Moreover, to capture lattice mismatch and thermal strain evolution, knowledge of the thermal expansion is necessary. Although there is plenty of results from measurements available in the literature, there is significant scatter among the reported data, which makes it highly uncertain. In fact, the reported data for δ-ZrH_x lies in the range $\sim 3 \cdot 10^{-6} - 30 \cdot 10^{-6}$ K^{-1} [49–54], which differ by approximately one order of magnitude. Thus, a reliable account of the thermal expansion is necessary for an accurate description of the thermally-induced strain behaviour in hydrides.

To address these issues, we perform a systematic theoretical investigation of the thermo-elastic properties of δ-ZrH_x and δ-TiH_x. To this end, we rely on DFT modelling within the QHA to incorporate finite temperature effects. Thus, the paper has two overarching objectives: (i) Investigate the thermal expansion of free-standing hydrides and (ii) establish the temperature dependent elastic constants to serve as input to describe the elastic strain energy for phase transformation modelling. Moreover, to gain insight into the roles of the governing mechanisms contributing to the thermally-induced variations of the elastic constants, we quantify the importance of different contributions to the reduction in stiffness.

The rest of the paper is organized as follows: in the next section we present the method, in which we detail the adopted hydride phase representation and utilized modelling strategy. This is followed by a presentation and discussion of the results. Finally, the key findings are summarized and conclusions are stated.

2. Method

2.1. Phase representation

For the non-stoichiometric δ-phase, the metallic ions are positioned in an FCC lattice with hydrogen randomly occupying tetrahedral interstitial sites. Thus, to account for the variation in hydrogen occupancy, the phase should ideally be represented by a large supercell. But because of the high computational cost associated with first-principles phonon calculations, we limited the study to $x = 1.5$ and adopted the crystallographic representation previously utilized in the literature [27,28,32,34,55–57], in which the phase is approximated as an ordered FCC alloy with all but two out of the eight tetrahedral interstitial sites being occupied by H. This enables the usage of a smaller supercell and improved symmetry exploitation, which is numerically beneficial when computing the phonon properties. Previous works [27,34] have shown that, of the three possible configurations, a ⟨100⟩ hydrogen divacancy leads to a crystal that is tetragonal, but very close to cubic under equilibrium conditions, see Fig. 1. In fact, the c/a ratio deviates by less than 1% from unity for both δ-$ZrH_{1.5}$ [34,55] and δ-$TiH_{1.5}$ [32,35,57] such that it for all practical purposes can be considered cubic, which is why it was deemed representative for the δ-phase and adopted herein.

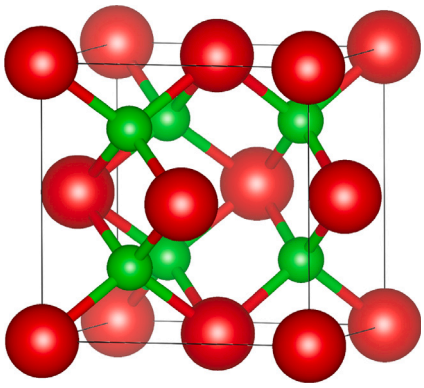

Fig. 1. δ-$MH_{1.5}$ representation. The red particles represent metallic ions and the green correspond to hydrogen.

In addition to the Zr and Ti hydrides, we also investigated the thermal expansion and thermal dependence of the elastic constants of α-Zr. This is motivated by the fact that there is an abundance of experimental data available in the literature, which was used to benchmark the modelling approach.

2.2. Thermo-elastic properties

To incorporate thermally induced effects on the mechanical properties by means of DFT modelling, we resorted to the QHA, in which Helmholtz free energy, F, is expressed as

$$F(T,V) = E_0(V) + F_{vib}(T,V) + F_{el}(T,V) \tag{1}$$

where E_0 is the ground-state energy, $V = V(T, \epsilon_{ij})$ is the temperature and strain dependent volume, while F_{vib} and F_{el} represent the vibrational and electronic free energies [38], respectively. Since F_{el} scales with the electron density at the Fermi level [38], which is relatively low for Zr and hydrides [34], we neglected it herein such that the only contribution to the free energy comes from the vibrational free energy. It can be derived from the phonon density of states, $g(\omega, V)$, through the relation

$$F_{vib}(T,V) = k_B T \int_0^\infty g(\omega,V) \ln\left[2\sinh\left(\frac{\hbar\omega}{2k_B T}\right)\right] d\omega \tag{2}$$

where the k_B and $\hbar$ represent the Boltzmann and Planck constants, respectively [38]. To investigate the roles of different contributions to the elastic constants we partitioned (1) into ground-state and vibrational contributions. Moreover, we separated the contributions of metallic and hydrogen phonons on the temperature dependent elastic properties through the following decomposition: $F_{vib} = F_{vib,H} + F_{vib,M}$, where the terms on the right-hand side were evaluated using projected phonon densities of states of hydrogen and metallic atoms, respectively. We also investigated the impact of zero-point energy (ZPE)

$$F_{ZPE}(V) = \frac{1}{2}\int_0^\infty g(\omega,V)\hbar\omega d\omega \tag{3}$$

on the elastic constants. Since it does not contain any explicit temperature dependence it mainly provided a shift in the elastic constants in the zero temperature limit.

2.2.1. Thermal expansion

To delineate the thermal expansion, it is necessary to identify the lattice parameters that minimize (1). Thus, for the HCP phase, we mapped how the free energy varied with the a and c lattice parameters to locate the minimum at for different temperatures. The thermal expansion coefficients were then computed as $\alpha_a = (1/a_{RT})da/dT$ and $\alpha_c = (1/c_{RT})dc/dT$, where a_{RT} and c_{RT} are the hexagonal reference lattice parameters at room temperature. Based on this data the averaged

Table 1
Applied strain combinations employed for extracting the elastic constants. The rightmost column represents the value of the square term in the expansion of Eq. (6).

	Strain combination	A_2
δ-$MH_{1.5}$	$\epsilon_{11}=\epsilon_{22}=\epsilon_{33}=\epsilon$	$3C_{11}+6C_{12}$
	$\epsilon_{11}=\epsilon_{22}=-\epsilon_{33}=\epsilon$	$3C_{11}-2C_{12}$
	$\epsilon_{12}=\epsilon_{23}=\epsilon_{13}=\epsilon$	$12C_{44}$
α-Zr	$\epsilon_{11}=\epsilon_{22}=\epsilon$	$2C_{11}+2C_{12}$
	$\epsilon_{11}=-\epsilon_{22}=\epsilon$	$2C_{11}-2C_{12}$
	$\epsilon_{11}=\epsilon_{22}=-\epsilon_{33}=\epsilon$	$2C_{11}+2C_{12}+C_{33}-4C_{13}$
	$\epsilon_{33}=\epsilon$	C_{33}
	$\epsilon_{13}=\epsilon$	$4C_{44}$

linear thermal expansion was defined as $\alpha_L=(2\alpha_a+\alpha_c)/3$ such that the volumetric expansion is $\alpha_V=3\alpha_L$.

It was found that mapping the lattice parameters in the range $0.99\leq a/a_0, c/c_0\leq 1.03$ with 13 increments, where a_0 and c_0 are the ground-state lattice parameters, was sufficient to describe the temperature dependence and thermal expansion of α-Zr accurately. Likewise, for the δ-phase the lattice parameter was varied between $1.0\leq a/a_0\leq 1.05$ in 20 increments.

2.2.2. Elastic constants

The isothermal elastic constants, C_{ijkl}, are defined as the second derivative of the volume specific Helmholtz free energy with respect to the applied strain, i.e.

$$C_{ijkl}=\frac{1}{V_0}\left(\frac{\partial^2 F}{\partial\epsilon_{ij}\partial\epsilon_{kl}}\right)_{\epsilon_{ij}=0} \tag{4}$$

where $V_0=V_0(T)$ represents the temperature dependent reference volume and ϵ_{ij} is the Green–Lagrange strain tensor. The strain tensor is connected to the deformation gradient, F_{ij}, through the relation

$$\epsilon_{ij}=\frac{1}{2}(F_{ki}F_{kj}-\delta_{ij}) \tag{5}$$

where δ_{ij} is the Kronecker delta and F_{ij} represents the linear mapping between the reference state, X_i, and the deformed state, x_i, i.e. $x_i=F_{ij}X_j$ [58].

In case of cubic symmetry, the number of independent elastic constants is reduced from 21 to three: C_{1111}, C_{1122} and C_{2323}, or C_{11}, C_{12} and C_{44} in Voigt notation [59], respectively. To extract them, we computed the strain energy as function of the applied strain for three linearly independent combinations of strain and calculated the second derivative according to Eq. (4). To this end we used three independent strain states, see Table 1. For the HCP phase there are five independent elastic constants: C_{11}, C_{12}, C_{13}, C_{33} and C_{44} [59]. We adopted the combinations of strain from [40], as indicated in Table 1, to compute them.

For each temperature, we evaluated the free energy by applying 13 equal strain increments in the range of −3% to 3% for each strain combination. The free energy was then fitted to a fourth order polynomial

$$\frac{F(\epsilon,T,V_0(T))}{V_0(T)}=A_0+A_1\epsilon+\frac{A_2}{2}\epsilon^2+\frac{A_3}{6}\epsilon^3+\frac{A_4}{24}\epsilon^4 \tag{6}$$

where the A_2-term comprised linear combinations of the elastic constants as indicated in Table 1.

To describe the elastic constants over a wide range of temperature, a semi-empirical expression, which has proven to be highly accurate at the low temperature regime, was derived by Varshni [60]:

$$C_{ijkl}(T)=C^0_{ijkl}-\frac{s_{ijkl}}{\exp(t_{ijkl}/T)-1} \tag{7}$$

where s, t and C^0 are material specific constants with the same symmetries as the second order elastic tensor. The theoretical derivation of Eq. (7) is based on an Einstein model of a solid [60], but its validity fails at elevated temperatures, where anharmonic effects become increasingly importants [61]. Eq. (7) can be expanded as

$$C_{ijkl}\approx C^0_{ijkl}-s_{ijkl}\left(\frac{T}{t_{ijkl}}-\frac{1}{2}+\frac{1}{12}\frac{t_{ijkl}}{T}+\cdots\right) \tag{8}$$

from which it is seen that elastic temperature dependence assumes a linear behaviour when $T\gg t$, in accordance with experimental observations, see e.g. [25,60,62–64]. When s is positive, a reduction in the elastic constant is observed with increasing temperature, but previous works have shown that s can be negative, which promotes an increase in the associated elastic constants with increasing temperature. Notably, such behaviour has been observed for s_{12} and/or s_{13} of HCP metals, e.g. α-Ti, α-Zr, α-Hf, α-Os, α-Zn and α-Cd [64–68].

2.3. Numerical details

For all DFT simulations in this work we have used the Vienna *ab initio* simulation package (VASP) [69–72]. The interaction between valence electrons and the core were described using standard pseudopotentials from the VASP library, generated with the projector augmented-wave (PAW) method [73,74]. For Zr and Ti, electron descriptions corresponding to the $4d^25s^2$ and $3d^24s^2$ valence states were employed, respectively, while only the $1s^1$ electron was treated for H. We chose the kinetic energy cutoff for the plane-wave basis set and k-point density such that the ground-state energy was well-converged. To achieve this, we used a kinetic energy cutoff of 520 eV and a k-point grid for the first Brillouin zone of the reciprocal hydride cell corresponding to a Γ-centred $12\times12\times12$ grid generated by means of the Monkhorst–Pack method [75]. Likewise, for the primitive cell of α-Zr, a $16\times16\times10$ k-point grid was utilized. For the calculations, we used smearing based on the Methfessel-Paxton method with a width corresponding to 0.1 eV [76]. The adopted exchange–correlation functional was described by the generalized gradient approximation using the parametrization of Perdew, Burke and Ernzerhof (PBE) [77,78].

For the phonon calculations, we adopted the finite difference method as implemented in the open source Phonopy software [79]. To this end we used $2\times2\times2$ and $4\times4\times2$ supercells for the δ- and α-Zr phases, respectively. These supercell sizes were found to be sufficiently large to produce well converged phonon density of states for the ground-state structures, see the Appendix.

3. Results and discussion

3.1. Thermal expansion

3.1.1. Zirconium matrix

As model benchmark we compare the thermally-induced lattice parameter variation and thermal expansion of α-Zr with measured data [80,81]. In Fig. 2(a) and (b) it is seen that the lattice parameters computed by means of DFT slightly overestimate the experimental data by up to a percent. This observed overestimation is in line with general observations for the PBE functional [82]. Evaluation of the linear thermal expansion coefficients, see Fig. 2(c), reveals that the average expansion coefficient matches experimental data well. Notably we observe an initially negative thermal expansion behaviour in the c-direction, which was previously seen in DFT calculations for α-Zr [40] and α-Ti [83]. These anisotropic tendencies, i.e. simultaneous thermally-induced expansion and compression in different directions, are believed to be associated with mode softening at the Brillouin zone boundary that emerges in connection compression of the c-axis [83]. Such behaviour may trigger negative Grüneisen parameters that give rise to a negative thermal expanding component in one of the lattice directions.

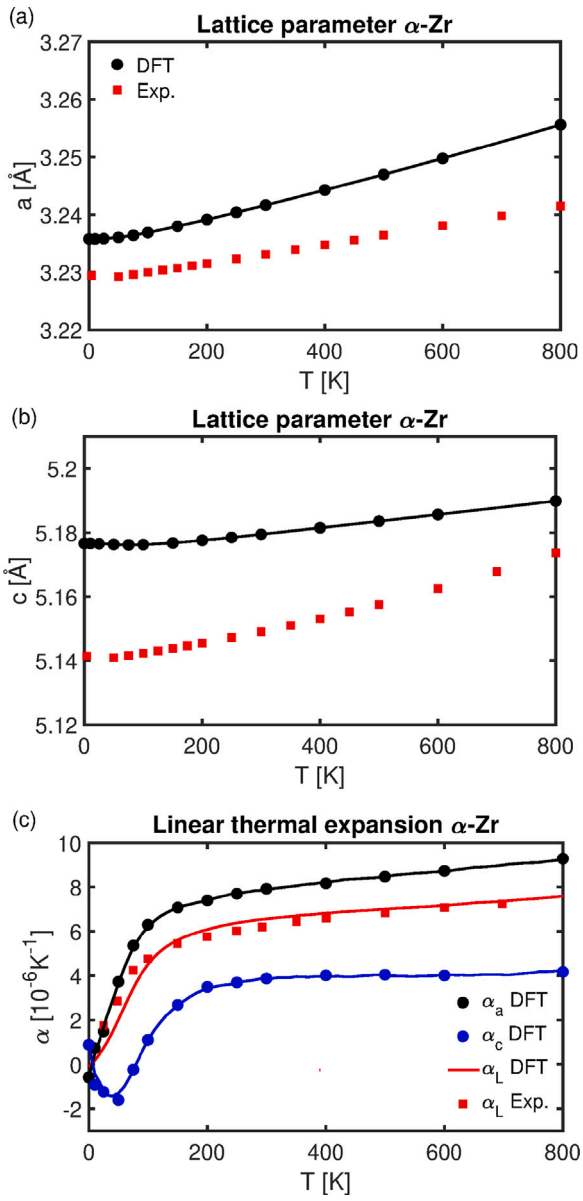

Fig. 2. Thermally-induced variation of the lattice parameters (a) a and (b) c for α-Zr, along with (c) the associated thermal expansion. The experimental data in (a) and (b) is taken from [80,81], respectively.

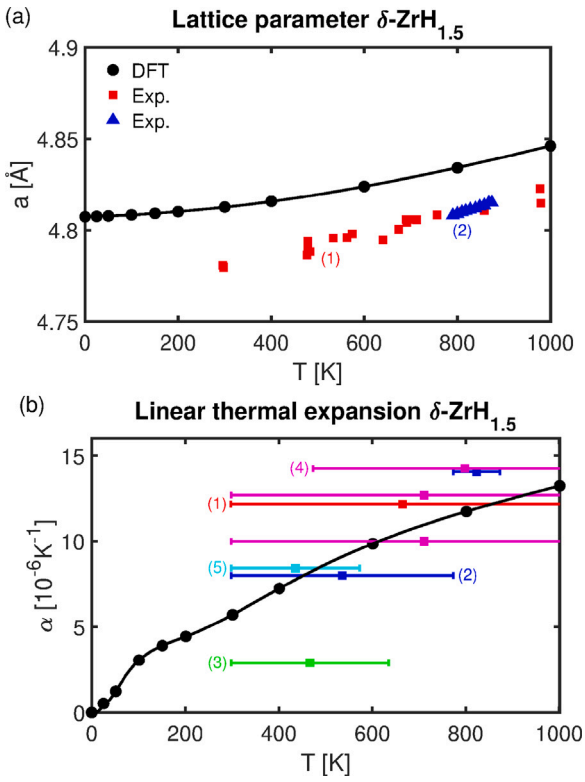

Fig. 3. (a) Thermally-induced variation of the lattice parameter and (b) the thermal expansion of $ZrH_{1.5}$. The experimental lattice parameters are for the stoichiometry ranges $1.60 < x < 1.70$. The experimental linear thermal expansion data for the hydrides are given as averages over a range of temperature that is indicated by the horizontal bars. The experimental data in the figure is from: (1) Moore et al. [51], (2) Cinbiz et al. [54], (3) Kempter et al. [49], (4) Beck [50] and (5) Yamanaka et al. [84].

3.1.2. Hydrides

For δ-$ZrH_{1.5}$, we similarly find that the computed lattice parameters overestimate those from experiments, see Fig. 3(a). In Fig. 3(b), we have computed the thermal linear expansion coefficient of δ-$ZrH_{1.5}$ along with results from experimental measurements. The linear thermal expansion coefficient is found to increase from zero up to $13.5 \cdot 10^{-6}$ K^{-1} at $T = 1000$ K. Comparison with the results in Fig. 2(c), this value corresponds to roughly twice that of the matrix.

When comparing with available experimental data there are some outliers. Most notably, the low value of $\alpha = 2.98 \cdot 10^{-6}$ K^{-1} from Kempter et al. [49] and the high value quoted from Yamanaka et al. [52] corresponding to $20 - 30 \cdot 10^{-6}$ K^{-1} (not shown in Fig. 3). However, as pointed out by Cinbiz et al. [54], it is not clear from [52] whether it is the linear or volumetric thermal expansion that is considered. In a follow-up paper [84], the authors referred to the same data as the volumetric thermal expansion coefficient, which would imply that the linear thermal expansion coefficient in fact lies in the range $6.6–10 \cdot 10^{-6}$ K^{-1} for the temperature range 300–600 K. This concurs fairly well with our DFT data, see Fig. 3(b).

We note that there is a variation in the thermal expansion coefficient values reported by Beck [50] and Cinbiz et al. [54], depending on the thermal range over which α was averaged. Some of these differences were attributed to the presence of other hydride morphologies (mainly γ-ZrH) than the δ-phase, which impact the thermal expansion [50,54]. To dissolve the other hydrides, high temperature measurements were required. Such measurements produced experimental values of $\sim 14 \cdot 10^{-6}$ K^{-1} at $T \sim 800$ K [50,54], which is slightly higher than our DFT data of $12 \cdot 10^{-6}$ K^{-1} at the same temperature. Overall, our results and the experimental data line up quite well, if the temperature range over which the thermal expansion coefficient was measured, i.e. the horizontal bars in Fig. 3(b), is taken into account. This would suggest that the impact of the γ-hydride indeed is quite small. It also implies that much of the reported discrepancy in the literature instead is related to the fact that the thermal expansion coefficient is highly temperature dependent, and that it is necessary to consider the relevant temperature interval to extract the accurate data.

Unlike the aforementioned phases, the optimal lattice parameter of δ-$TiH_{1.5}$ underestimates the available experimental data [85,86], see Fig. 4(a). Despite typical underbinding tendencies associated with PBE [82], such behaviour has been reported previously [32,35] when performing DFT modelling of titanium hydrides. We also note that the hydrogen content associated with the experimental data is higher ($1.75 < x < 1.92$) than we have considered herein ($x = 1.5$), which is expected to produce a somewhat larger lattice parameter and could explain the observed discrepancy.

Concerning the thermal expansion, which has been reported in the literature to be independent of the hydrogen content [86], we find that

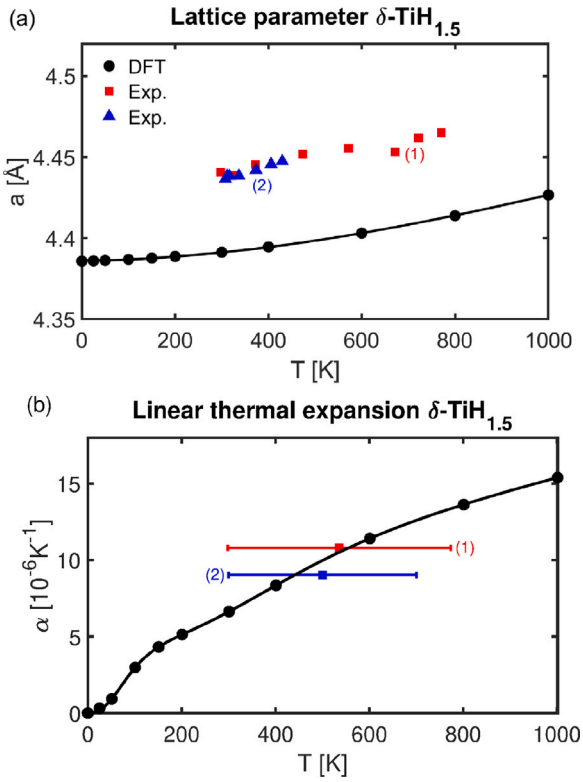

Fig. 4. (a) Thermally-induced variation of the lattice parameter and (b) the thermal expansion of $TiH_{1.5}$. The experimental lattice parameters and thermal expansions are for the stoichiometry range $1.75 < x < 1.92$ from: (1) Yakel Jr. [85] and (2) Setoyama et al. [86].

Table 2
Parameters associated with fits to the Varshni relation, Eq. (7). The parameters C^0 and s are given in the unit of GPa and t is given in K.

	α-Zr (DFT)	α-Zr (Exp.)	δ-$ZrH_{1.5}$ (DFT)	δ-$TiH_{1.5}$ (DFT)
C^0_{11}	146	155	147	171
s_{11}	6.83	5.46	18.1	11.6
t_{11}	93.2	111	789	431
C^0_{12}	69.3	67.2	113	111
s_{12}	−4.08	−2.62	10.5	13.4
t_{12}	111	120	472	568
C^0_{33}	162	173	–	–
s_{33}	5.94	4.29	–	–
t_{33}	109	132	–	–
C^0_{13}	70.1	64.6	–	–
s_{13}	−12.9	−0.05	–	–
t_{13}	2136	25.4	–	–
C^0_{44}	26.6	36.3	52.4	55.7
s_{44}	2.42	0.554	11.7	16.5
t_{44}	129	37.4	1401	1659

the experimental data matches quite well with our computed DFT data, see Fig. 4(b).

3.2. Temperature dependent elastic properties

3.2.1. Zirconium matrix

As benchmark we have computed the isothermal elastic constants for α-Zr in Fig. 5(a). The resulting data reveal an overall good agreement with measured data, with most observed experimental trends captured by the modelling. Several of the elastic constants (C_{11}, C_{33} and C_{44}) underestimate the experimental data by approximately 10 GPa in the zero temperature limit, which is of the order of agreement that can be expected for DFT modelling. The remaining elastic constants deviate

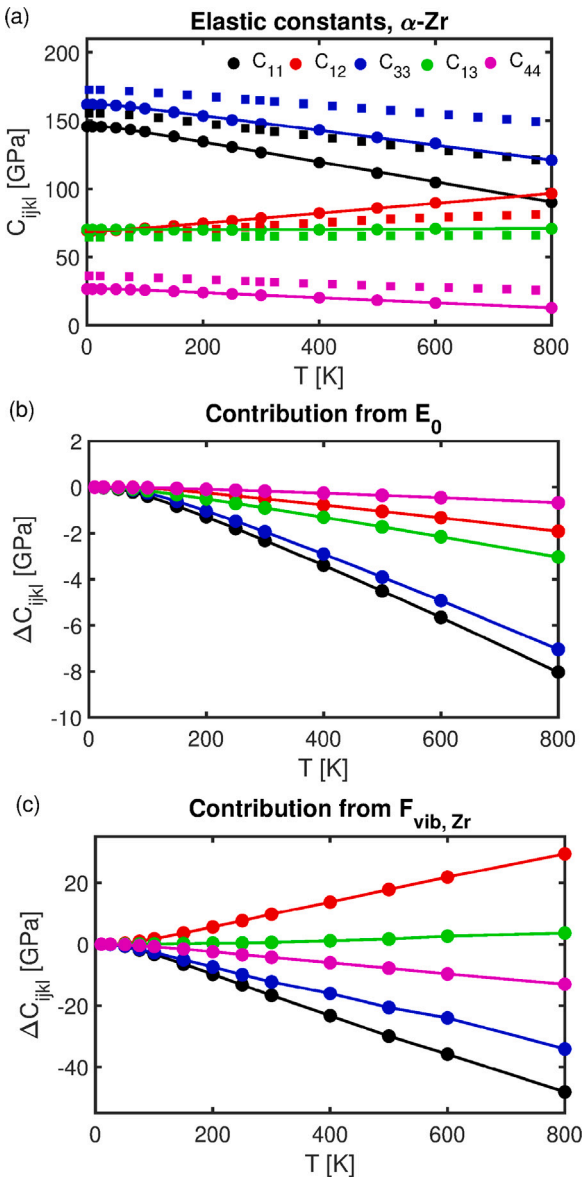

Fig. 5. (a) Thermo-elastic constants of α-Zr – the circular markers represent DFT data and the solid lines correspond to fits to the Varshni-relation, while the square markers are experimental data [64]. Variations from individual contributions to the total elastic constants from (b) the ground-state energy and (c) vibrational free energy.

less from experimental data in the low temperature limit. The resulting Varshni parameters are given in Table 2. We note that most computed s and t values differ a lot from experimental values. But by comparing the s/t-ratios, it is seen that they agree well. Thus, based on the series expansion (8), it can be concluded that the high temperature behaviour is captured by the DFT data.

In line with previous experimental and DFT results for α-Zr and α-Ti [40,43,64], we find that C_{12} increases with increasing temperature, while C_{13} remains fairly constant. We note that these increasing trends for isothermal elastic constants were not obtained for local density approximated DFT calculations of α-Zr in [40], where both C_{12} and C_{13} were found to be more or less independent of the temperature. But by transforming from isothermal to adiabatic elastic constants, such trends could be seen.

Decomposition of the different contributions to the free energy reveal their relative importance to the thermal dependence. In Fig. 5(b) the impact of the ground-state energy contribution on the thermal

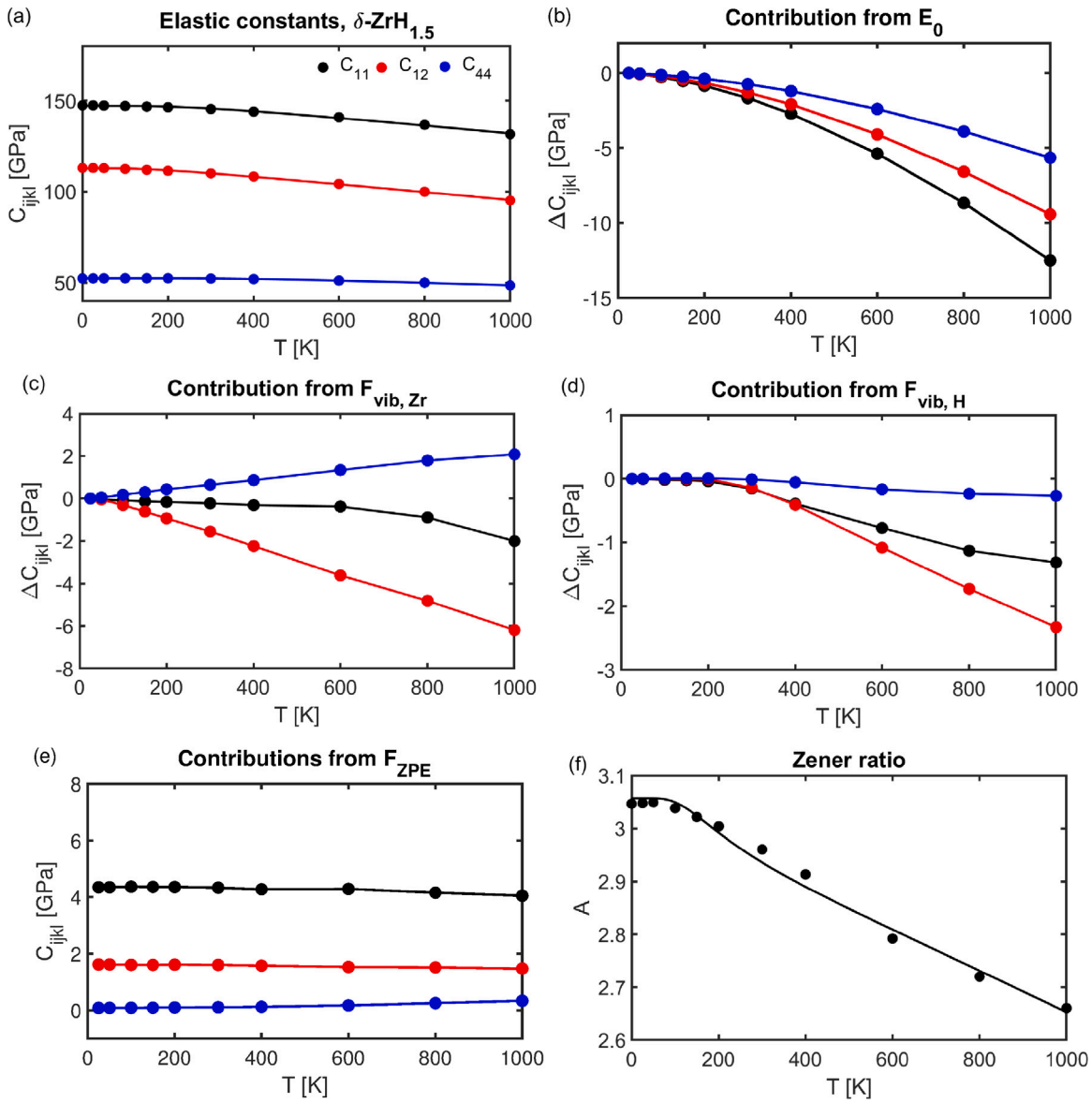

Fig. 6. (a) Thermo-elastic constants of δ-$Zr_{1.5}$ – the circular markers represent DFT data and the solid lines correspond to fits to the Varshni-relation. Variations from individual contributions to the total elastic constants from (b) the ground-state energy, vibrational free energy derived from (c) Zr and (d) H phonons and (e) zero point energy. (f) Temperature dependence of the Zener ratio.

dependence on the elastic constants is given. The simplification of neglecting the vibrational contribution to the total free energy (Eq. (1)) corresponds to so-called quasi-static approach outlined in [87], where finite temperature effects are incorporated as part of the thermal expansion only. It is seen that the ground-state energy contribution to the elastic constants give rise to reductions in the stiffness that are relatively small. The most significant reduction is found for C_{11}, and it corresponds to only 8 GPa over a temperature range of 800 K. The impact of vibrational free energy on the elastic constants is much more significant, see Fig. 5(c). It can contribute to elastic constants either increasing or decreasing by as much as 50 GPa over an 800 K temperature range, which is much more than predicted by the quasi-static approach. Thus, the vibrational free energy is critical to describe the elastic constants of α-Zr.

3.2.2. Hydrides

In Figs. 6 and 7 the elastic constants for δ-$ZrH_{1.5}$ and δ-$TiH_{1.5}$ are presented, respectively, along with the associated Varshni parameters in Table 2. Generally, they are found not to vary as much with temperature as the matrix, since none of them reduce by more than 25 GPa over the temperature range $0 \leq T \leq 1000$ K. These tendencies concur with the observations from nanoindentation experiments of Zr [25,26], where the s/t-ratio for Young's modulus of the matrix was found to be approximately three times higher than for the hydride.

Unlike the matrix, the majority of the thermally-induced reduction of the elastic constants can be attributed to strain-induced variations in the ground-state energy, see Figs. 6(b) and 7(b). Inspection of contributions of the projected phonon densities of state on the elastic constants reveals that generally the metallic ions have a larger impact of the thermal dependence than the hydrogen atoms, see Figs. 6(c–d) and 7(c–d). It is, however, noted that their combined impact sums up to less than 10 GPa over the range of 1000 K. For C_{11} this contribution to the free energy is responsible for less than 25% of the thermally-induced reduction, while for C_{12} it constitutes up to 50%.

Because any temperature dependent effects on the ZPE, only occur indirectly via the induced volume expansion, it does not contribute

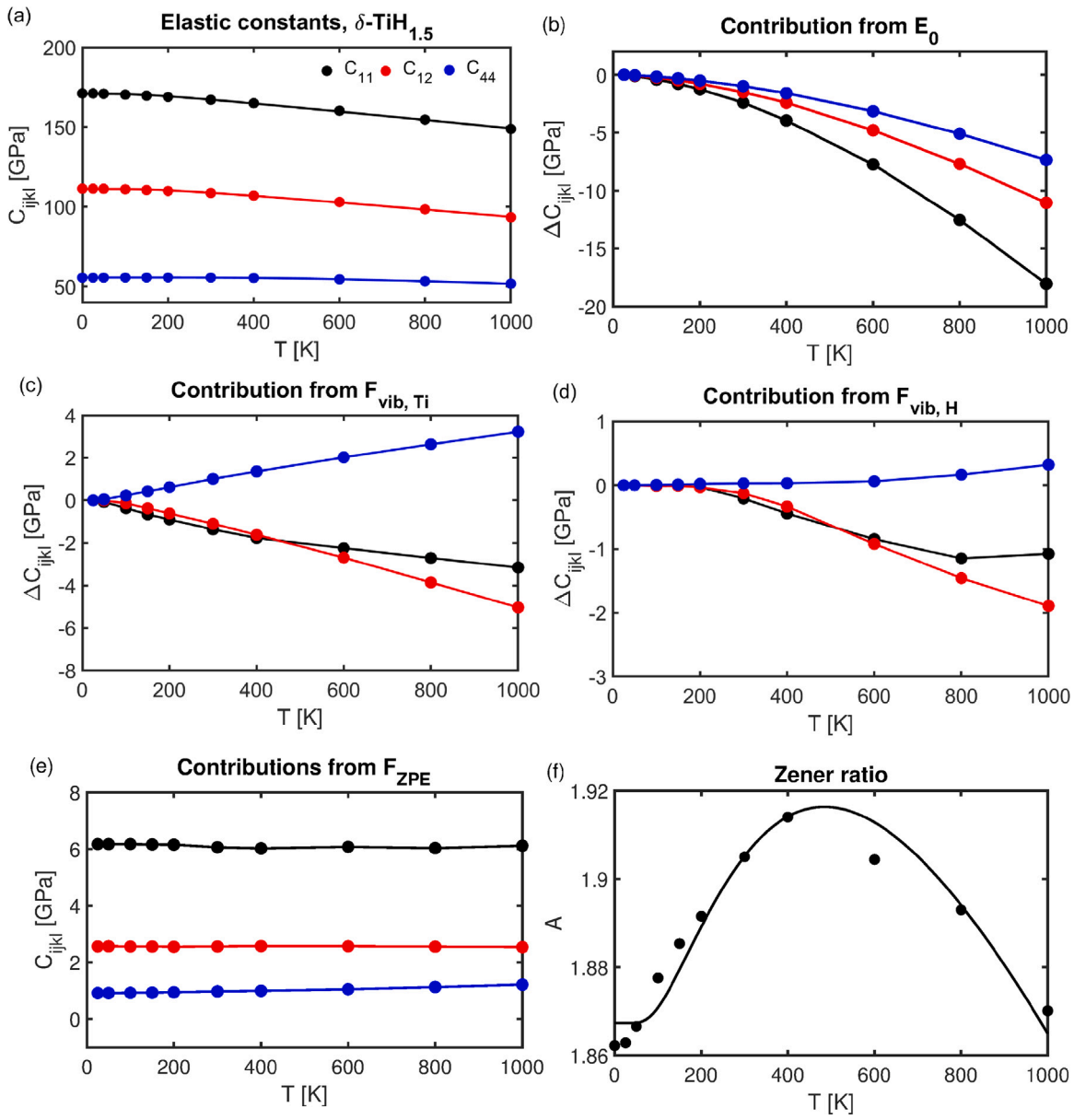

Fig. 7. (a) Thermo-elastic constants of δ-$Ti_{1.5}$ – the circular markers represent DFT data and the solid lines correspond to fits to the Varshni-relation. Variations from individual contributions to the total elastic constants from (b) the ground-state energy, vibrational free energy derived from (c) Zr and (d) H phonons and (e) zero point energy. (f) Temperature dependence of the Zener ratio.

to elastic constants varying with temperature, see Figs. 6(e) and 7(e). Instead, it gives rise to a static shift, which for the hydrides considered herein is up to 6 GPa. Thus, although it seems to lack predictability to compute the elastic constants for α-Zr, in light of the relatively low impact of the vibrational free energy on the elastic constants of hydrides, these findings suggest that the proposed DFT-based quasi-static approach of Wang et al. [87], may yield satisfactory results.

As a final result, we present the Zener anisotropy ratio

$$A = \frac{2C_{44}}{C_{11} - C_{12}} \tag{9}$$

for the hydrides and how it varies with temperature, see Figs. 6(f) and 7(f). For the titanium hydride, it is seen that A remains fairly constant at $\sim$ 1.9 over the considered temperature range. The anisotropy ratio is higher for δ-$ZrH_{1.5}$, corresponding to $\sim$ 3 at low temperature, while reducing to $\sim$ 2.6 at elevated temperatures. Thus, a thermally-induced change in the Zener ratio occurs, which suggests that the elastic anisotropy has a temperature dependence.

4. Summary and conclusions

In the present work, we have studied the thermal expansion and temperature dependent elastic constants of δ-$ZrH_{1.5}$ and δ-$TiH_{1.5}$ by means of DFT modelling conducted within the QHA. This aims to clarify the elastic anisotropy of hydrides and provide input data for phase transformation modelling of hydride precipitation.

The computed thermal expansion varies from 0 up to about $13.5 \cdot 10^{-6}$ and $15 \cdot 10^{-6}$ K^{-1} for δ-$ZrH_{1.5}$ and δ-$TiH_{1.5}$, respectively, over the temperature range spanning from 0 to 1000 K. With the exception of some outliers reported in the literature, these results concur well with available experimental data. Compared with the computed data for α-Zr, we find that the linear thermal expansion for hydrides is roughly twice that of the matrix at elevated temperature.

Finally, we investigate the temperature dependent elastic properties. In agreement with tendencies observed experimentally for Young's modulus, we find that any temperature-induced variations in the elastic

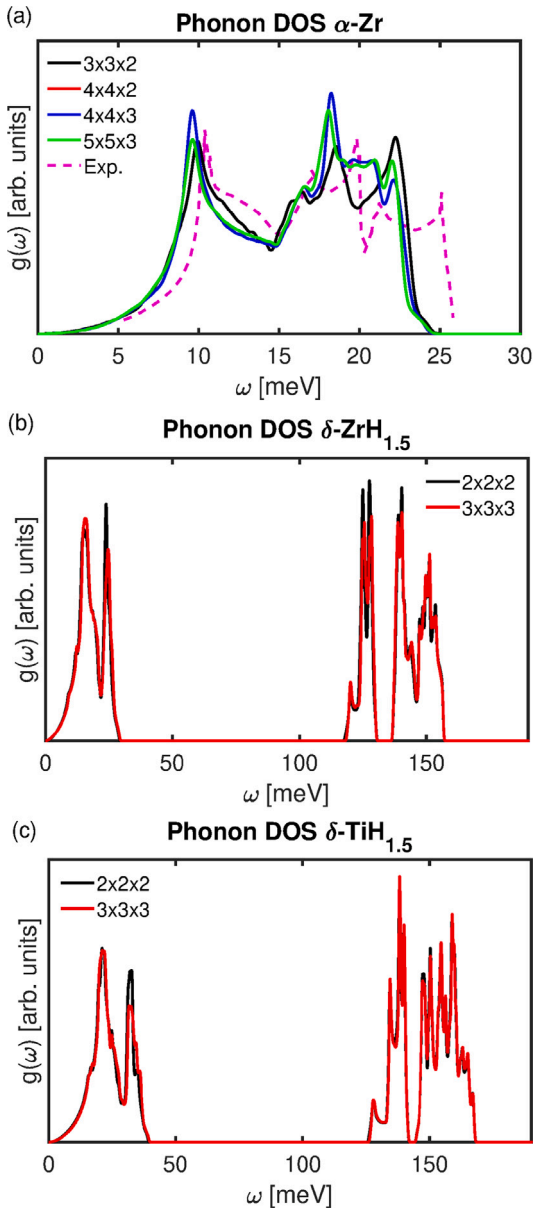

Fig. A.1. Computed phonon DOS for (a) α-Zr, (b) δ-$ZrH_{1.5}$ and (c) δ-$TiH_{1.5}$ for different supercell sizes. We note that the $4 \times 4 \times 2$ (red) and $4 \times 4 \times 3$ (blue) curves overlap. The experimental data in (a) is taken from [88].

constants are much more significant for the matrix than for the hydrides. For the hydrides, the most dominant contributor to the observed increased compliance emanates from volume-induced variations in the ground-state energy, while the impact of the vibrational free energy impacts the elastic constants to a lesser degree. In contrast, for α-Zr we find that the opposite tendencies are observed. For the δ-$ZrH_{1.5}$ phase, we find that the Zener ratio varies with temperature, which suggests that the elastic anisotropy is temperature dependent. Such tendencies were not found for δ-$TiH_{1.5}$.

CRediT authorship contribution statement

Pär A.T. Olsson: Conceptualization, Methodology, Modelling, Formal analysis, Writing – original draft, Review and editing, Funding acquisition.

Declaration of competing interest

The authors declare that they have no known competing financial interests or personal relationships that could have appeared to influence the work reported in this paper.

Data availability

Data will be made available on reasonable request.

Acknowledgements

This work was funded by the Swedish Research Council through grant no. 2016-04162 and the Swedish Knowledge Foundation through grant no. 2013-0022. The author wishes to acknowledge the Swedish National Infrastructure for Computing (SNIC) at the National Supercomputer Centre (NSC), Linköping University and at the High Performance Computing Center North (HPC2N), Umeå University for providing the computational resources needed to conduct this study.

Appendix. Phonon densities of states

In Fig. A.1 we have compiled the results from the phonon density of states (DOS) convergence study for the α-Zr, δ-$ZrH_{1.5}$ and δ-$TiH_{1.5}$ phases. For the former, it is seen that a converged DOS profile can be obtained for a supercell comprising a $4 \times 4 \times 2$ grid. Although, we note that experimental frequencies lie in a somewhat higher energy band than the DFT data, the majority of the characteristics are captured by the computed phonons. Hence, we adopted a $4 \times 4 \times 2$ supercell for the α-Zr phonon calculations.

For the hydrides it is found that a $2 \times 2 \times 2$ unit cell grid provides converged results compared to the phonon DOS of $3 \times 3 \times 3$ supercells. Thus, we used $2 \times 2 \times 2$ supercells to compute the phonon DOS of the hydrides.

References

[1] M.P. Puls, The effect of Hydrogen and Hydrides on the Integrity of Zirconium Alloy Components, first ed., Springer, 2012.
[2] R.R. Boyer, Titanium for aerospace: rationale and applications, Adv. Perform. Mater. 2 (1995) 349–368.
[3] E.O. Ezugwu, J. Bonney, Y. Yamane, An overview of the machinability of aeroengine alloys, J. Mater Process. Technol. 134 (2003) 233–253.
[4] R.R. Boyer, Attributes, characteristics, and applications of titanium and its alloys, JOM 65 (2010) 21–24.
[5] E. Zuzek, J.P. Abriata, A. San-Martin, F.D. Manchester, H-Zr (Hydrogen-Zirconium), in: F.D. Manchester (Ed.), Phase Diagrams of Binary Hydrogen Alloys, ASM International, Materials Park, Ohio, USA, 2000, pp. 309–322.
[6] F.D. Manchester, A. San-Martin, H-Ti (Hydrogen-Titanium), in: F.D. Manchester (Ed.), Phase Diagrams of Binary Hydrogen Alloys, ASM International, Materials Park, Ohio, USA, 2000, pp. 238–258.
[7] D.O. Northwood, U. Kosasih, Hydrides and delayed hydrogen cracking in zirconium and its alloys, Int. Met. Rev. 28 (1983) 92–121.
[8] R.R. Boyer, W.F. Spurr, Characteristics of sustained-load cracking and hydrogen effects in Ti-6Al-4V, Metall. Trans. A 9A (1978) 23–29.
[9] C. Cann, E. Sexton, An electron optical study of hydride precipitation and growth at crack tips in zirconium, Acta Metall. 28 (1980) 1215–1221.
[10] D. Shih, I. Robertson, H. Birnbaum, Hydrogen embrittlement of α-titanium: *In situ* TEM studies, Acta Metall. 36 (1) (1988) 111–124.
[11] J. Bair, M. Asle Zaeem, M. Tonks, A review on hydride precipitation in zirconium alloys, J. Nucl. Mater. 466 (2015) 12–20.
[12] A.T. Motta, L. Capolungo, L.-Q. Chen, M.N. Cinbiz, M.R. Daymond, D.A. Koss, E. Lacroix, G. Pastore, P.-C.A. Simon, M.R. Tonks, B.D. Wirth, M.A. Zikry, Hydrogen in zirconium alloys: A review, J. Nucl. Mater. 518 (2019) 440–460.
[13] E. Conforto, I. Guillot, X. Feaugas, Solute hydrogen and hydride phase implications on the plasticity of zirconium and titanium alloys: a review and some recent advances, Philos. Trans. Royal Soc. A 375 (2017) 20160417.
[14] X. Zhu, D.-Y. Lin, J. Fang, X.-Y. Gao, Y.-F. Zhao, H.-F. Song, Structure and thermodynamic properties of zirconium hydrides by structure search method and first principles calculations, Comput. Mater. Sci. 150 (2018) 77–85.
[15] Z. Zhao, J.-P. Morniroli, A. Legris, A. Ambard, Y. Khin, L. Legras, M. Blat-Yrieix, Identification and characterization of a new zirconium hydride, J. Microsc. 232 (2008) 410–421.

[16] L. Thuinet, A. De Backer, A. Legris, Phase-field modeling of precipitate evolution dynamics in elastically inhomogeneous low-symmetry systems: Application to hydride precipitation in Zr, Acta Mater. 60 (2012) 5311–5321.
[17] J. Bair, M. Asle Zaeem, D. Schwen, Formation path of δ hydrides in zirconium by multiphase field modeling, Acta Mater. 123 (2017) 235–244.
[18] A. Toghraee, J. Bair, M. Asle Zaeem, Effects of applied load on formation and reorientation of zirconium hydrides: A multiphase field modeling study, Comput. Mater. Sci. 192 (2021) 110367.
[19] P.-C. Simon, L.K. Aagesen, A.M. Jokisaari, L.-Q. Chen, M.R. Daymond, A.T. Motta, M.R. Tonks, Investigation of δ zirconium hydride morphology in a single crystal using quantitative phase field simulations supported by experiments, J. Nucl. Mater. 557 (2021) 153303.
[20] A.R. Massih, Second-phase nucleation on an edge dislocation, Phil. Mag. 91 (2011) 3961–3980.
[21] L.O. Jernkvist, A.R. Massih, Multi-field modelling of hydride forming metals. Part I: Model formulation and validation, Comput. Mater. Sci. 85 (2014) 363–382.
[22] L.O. Jernkvist, Multi-field modelling of hydride forming metals Part II: Application to fracture, Comput. Mater. Sci. 85 (2014) 383–401.
[23] C.F. Nigro, C. Bjerkén, P.A.T. Olsson, Phase structural ordering kinetics of second-phase formation in the vicinity of a crack, Int. J. Fract. 209 (2018) 91–107.
[24] W. Reheman, P. Ståhle, M. Fisk, R. Singh, On the formation of expanding crack tip precipitates, Int. J. Fract. 217 (2019) 35–48.
[25] K. Kese, P.A.T. Olsson, A.-M. Alvarez Holston, E. Broitman, High temperature nanoindentation hardness and Young's modulus measurement in a neutron-irradiated fuel cladding material, J. Nucl. Mater. 487 (2017) 113–120.
[26] M.N. Cinbiz, M. Balooch, X. Hu, A. Amroussia, K. Terrani, Nanoindentation study of bulk zirconium hydrides at elevated temperatures, J. Alloys Compd. 726 (2017) 41–48.
[27] C. Domain, R. Besson, A. Legris, Atomic-scale Ab-initio study of the Zr-H system: I. Bulk properties, Acta Mater. 50 (2002) 3513–3526.
[28] W. Zhu, R. Wang, G. Shu, P. Wu, H. Xiao, First-principles study of different polymorphs of crystalline zirconium hydride, J. Phys. Chem. C 114 (2010) 22361–22368.
[29] P. Zhang, B.-T. Wang, C.-H. He, P. Zhang, First-principles study of ground state properties of ZrH_2, Comput. Mater. Sci. 50 (2011) 3297–3302.
[30] X. Liu, B. Tang, Y. Zhang, Ab initio calculations of structure and thermodynamic properties of tetragonal-TiH_2 under high temperatures and pressures, Eur. Phys. J. Appl. Phys. 64 (2013) 10201.
[31] J. Liang, Y. Dai, L. Yang, S. Peng, K. Fan, X. Long, X. Zhou, X. Zu, F. Gao, Ab initio study of helium behavior in titanium tritides, Comput. Mater. Sci. 69 (2013) 107–112.
[32] C.P. Liang, H.R. Gong, Atomic structure, mechanical quality, and thermodynamic property of TiH_x phases, J. Appl. Phys. 114 (2013) 043510.
[33] H. Wang, A. Chroneos, C. Jiang, U. Schwingenschlögl, Modelling zirconium hydrides using the special quasirandom structure approach, Phys. Chem. Chem. Phys. 15 (2013) 7599–7603.
[34] P.A.T. Olsson, A.R. Massih, J. Blomqvist, A.-M. Alvarez Holston, C. Bjerkén, Ab initio thermodynamics of zirconium hydrides and deuterides, Comput. Mater. Sci. 86 (2014) 211–222.
[35] P.A.T. Olsson, J. Blomqvist, C. Bjerkén, A.R. Massih, Ab initio thermodynamics investigation of titanium hydrides, Comput. Mater. Sci. 97 (2015) 263–275.
[36] P.F. Weck, E. Kim, V. Tikare, J.A. Mitchell, Mechanical properties of zirconium alloys and zirconium hydrides predicted from density functional perturbation theory, Dalton Trans. 44 (2015) 18769–18779.
[37] J. Zheng, X. Zhou, L. Mao, H. Zhang, J. Liang, L. Sheng, S. Peng, First-principles study of the relative stability of various zirconium hydrides using the special quasirandom structures approach, Int. J. Hydrog. Energy 40 (2015) 4597–4604.
[38] S. Baroni, P. Giannozzi, E. Isaev, Density-functional perturbation theory for quasi-harmonic calculations, Rev. Mineral. Geochem. 71 (2010) 39–57.
[39] H.H. Pham, M.E. Williams, P. Mahaffey, M. Radovic, R. Arroyave, T. Cagin, Finite-temperature elasticity of fcc Al: Atomistic simulations and ultrasonic measurements, Phys. Rev. B 84 (2011) 064101.
[40] P.A.T. Olsson, First principles investigation of the finite temperature dependence of the elastic constants of zirconium, magnesium and gold, Comput. Mater. Sci. 99 (2015) 361–372.
[41] C. Malica, A. Dal Corso, Quasi-harmonic thermoelasticity of palladium, platinum, copper, and gold from first principles, J. Phys.: Condens. Matter 33 (2021) 475901.
[42] K. Kádas, L. Vitos, R. Ahuja, B. Johansson, J. Kollár, Temperature-dependent elastic properties of α-beryllium from first principles, Phys. Rev. B 76 (2007) 235109.
[43] U. Argaman, G. Makov, First-principles study of the temperature dependence of the elastic constants of hcp titanium, Comput. Mater. Sci. 184 (2020) 109917.
[44] T. Shao, B. Wen, R. Melnik, S. Yao, Y. Kawazoe, Y. Tian, Temperature dependent elastic constants for crystals with arbitrary symmetry: Combined first principles and continuum elasticity theory, J. Appl. Phys. 111 (2012) 083525.
[45] G.J. Ackland, X. Huang, K.M. Rabe, First-principles thermodynamics of transition metals: W, NiAl, and PdTi, Phys. Rev. B 68 (2003) 214104.
[46] D. Dragoni, D. Ceresoli, N. Marzari, Thermoelastic properties of α-iron from first-principles, Phys. Rev. B 91 (2015) 104105.
[47] M. Destefanis, C. Ravoux, A. Cossard, A. Erba, Thermo-elasticity of materials from quasi-harmonic calculations, Minerals 9 (2019) 16.
[48] P. Nath, J.J. Plata, J. Santana-Andreo, E.J. Blancas, A.M. Márquez, J. Fernández Sanz, High-throughput screening of the thermoelastic properties of ultrahigh-temperature ceramics, ACS Appl. Mater. Interfaces 13 (25) (2021) 29843–29857.
[49] C.P. Kempter, R.O. Elliott, K.A. Gschneidner, Thermal expansion of delta and epsilon zirconium hydrides, Chem. Phys. 33 (1960) 837–840.
[50] R.L. Beck, Research and Development of Metal Hydrides - Summary Report for October 1, 1958-September 30, 1960, Report (Denver, Colorado, US), 1960.
[51] K.E. Moore, W.A. Young, Phase studies of the Zr-H system at high hydrogen concentrations, J. Nucl. Mater. 27 (1968) 316–324.
[52] S. Yamanaka, K. Yoshioka, M. Uno, M. Katsura, H. Anada, T. Matsuda, S. Kobayashi, Thermal and mechanical properties of zirconium hydride, J. Alloys Compd. 293–295 (1999) 23–29.
[53] S. Yamanaka, K. Yamada, K. Kurosaki, M. Uno, K. Takeda, H. Anada, T. Matsuda, S. Kobayashi, Characteristics of zirconium hydride and deuteride, J. Alloys Compd. 330–332 (2002) 99–104.
[54] M.N. Cinbiz, X. Hu, K. Terrani, Thermal expansion behavior of δ-zirconium hydrides: Comparison of δ hydride powder and platelets, J. Nucl. Mater. 509 (2018) 566–576.
[55] P.A.T. Olsson, K. Kese, M. Kroon, A.-M. Alvarez Holston, Ab initio-based fracture toughness estimates and transgranular traction-separation modelling of zirconium hydrides, Modell. Simul. Mater. Sci. Eng. 23 (2015) 045015.
[56] J. Wormald, M. Zerkle, J. Holmes, Generation of the TSL for zirconium hydrides from Ab initio methods, J. Nucl. Engng. 2 (2021) 105–113.
[57] P.A.T. Olsson, M. Mrovec, M. Kroon, First principles characterisation of brittle transgranular fracture of titanium hydrides, Acta Mater. 118 (2016) 362–373.
[58] N.S. Ottosen, M. Ristinmaa, The Mechanics of Constitutive Modeling, first ed., Elsevier, 2005.
[59] M.A. Meyers, K.K. Chawla, Mechanical Behavior of Materials, Prentice-Hall, Upper Saddle River, NJ, 1999.
[60] Y.P. Varshni, Temperature dependence of the elastic constants, Phys. Rev. B 2 (1970) 3952–3958.
[61] G. Grimvall, Thermophysical Properties of Materials, North Holland, 1999.
[62] J. Tallon, A. Wolfenden, Temperature dependence of the elastic constants of aluminum, J. Phys. Chem. Solids 40 (1979) 831–837.
[63] J.B. Wachtman, W.E. Tefft, D.G. Lam, C.S. Apstein, Exponential temperature dependence of Young's modulus for several oxides, Phys. Rev. 122 (1961) 1754–1759.
[64] E.S. Fisher, C.J. Renken, Single-crystal elastic moduli and the hcp → bcc transformation in Ti, Zr, and Hf, Phys. Rev. 135 (1964) A482–A494.
[65] C. Pantea, I. Stroe, H. Ledbetter, J.B. Betts, Y. Zhao, L.L. Daemen, H. Cynn, A. Migliori, Elastic constants of osmium between 5 and 300 K, Phys. Rev. B 80 (2009) 024112.
[66] C.W. Garland, R. Dalven, Elastic constants of zinc from 4.2°K to 77.6°K, Phys. Rev. 111 (1958) 1232–1234.
[67] C.W. Garland, J. Silverman, Elastic constants of cadmium from 4.2°K to 300°K, Phys. Rev. 119 (1960) 1218–1222.
[68] G. Alers, J. Neighbours, The elastic constants of zinc between 4.2° and 670°K, J. Phys. Chem. Solids 7 (1958) 58–64.
[69] G. Kresse, J. Hafner, *Ab initio* molecular dynamics for liquid metals, Phys. Rev. B 47 (1993) 558–561.
[70] G. Kresse, J. Hafner, *Ab initio* molecular-dynamics simulation of the liquid-metal amorphous-semiconductor transition in germanium, Phys. Rev. B 49 (1994) 14251–14269.
[71] G. Kresse, J. Furthmüller, Efficient iterative schemes for *ab initio* total-energy calculations using a plane-wave basis set, Phys. Rev. B 54 (1996) 11169–11186.
[72] G. Kresse, J. Furthmüller, Efficiency of ab-initio total energy calculations for metals and semiconductors using a plane-wave basis set, Comput. Mater. Sci. 6 (1996) 15–50.
[73] P.E. Blöchl, Projector augmented-wave method, Phys. Rev. B 50 (1994) 17953–17979.
[74] G. Kresse, D. Joubert, From ultrasoft pseudopotentials to the projector augmented-wave method, Phys. Rev. B 59 (1999) 1758–1775.
[75] H.J. Monkhorst, J.D. Pack, Special points for Brillouin-zone integrations, Phys. Rev. B 13 (1976) 5188–5192.
[76] M. Methfessel, A.T. Paxton, High-precision sampling for Brillouin-zone integration in metals, Phys. Rev. B 40 (1989) 3616–3621.
[77] J.P. Perdew, K. Burke, M. Ernzerhof, Generalized gradient approximation made simple, Phys. Rev. Lett. 77 (1996) 3865–3868.
[78] J.P. Perdew, K. Burke, M. Ernzerhof, Generalized gradient approximation made simple [Erratum], Phys. Rev. Lett. 78 (1997) 1396.
[79] A. Togo, I. Tanaka, First principles phonon calculations in materials science, Scr. Mater. 108 (2015) 1–5.
[80] J. Goldak, L.T. Lloyd, C.S. Barrett, Lattice parameters, thermal expansions, and Grüneisen coefficients of Zirconium, 4.2 to 1130°K, Phys. Rev. 144 (1966) 478–484.
[81] D.E. Gray, American Institute of Physics Handbook, third ed., McGraw-Hill, 1972.

[82] P. Haas, F. Tran, P. Blaha, Calculation of the lattice constant of solids with semilocal functionals, Phys. Rev. B 79 (2009) 085104.
[83] U. Argaman, E. Eidelstein, O. Levy, G. Makov, Ab initio study of the phononic origin of negative thermal expansion, Phys. Rev. B 94 (2016) 174305.
[84] S. Yamanaka, K. Yamada, K. Kurosaki, M. Uno, K. Takeda, H. Anada, T. Matsuda, S. Kobayashi, Thermal properties of zirconium hydride, J. Nucl. Mater. 294 (2001) 94–98.
[85] H.L. Yakel Jr., Thermocrystallography of higher hydrides of titanium and zirconium, Acta Crystallogr. 11 (1958) 46–51.
[86] D. Setoyama, J. Matsunaga, H. Muta, M. Uno, S. Yamanaka, Mechanical properties of titanium hydride, J. Alloys Compd. 381 (2004) 215–220.
[87] Y. Wang, J.J. Wang, H. Zhang, V.R. Manga, S.L. Shang, L.-Q. Chen, Z.-K. Liu, A first-principles approach to finite temperature elastic constants, J. Phys. Cond. Matter 22 (2010) 225404.
[88] C. Stassis, J. Zarestky, D. Arch, O.D. McMasters, B.N. Harmon, Temperature dependence of the normal vibrational modes of hcp Zr, Phys. Rev. B 18 (1978) 2632–2642.